JOURNAL OF AIRCRAFT
Vol. 33, No. 1, January–February 1996

Integrated Structural Tailoring and Control Using Adaptive Materials for Advanced Aircraft Wings

L. Librescu,* L. Meirovitch,† and O. Song‡
Virginia Polytechnic Institute and State University, Blacksburg, Virginia 24061

This study combines structural tailoring with the adaptive capabilities of piezoelectric materials for the purpose of controlling the vibration and static aeroelastic characteristics of advanced aircraft wings. The structural model consists of a thin/thick-walled closed cross-sectional cantilevered beam whose constituent layers exhibit elastic anisotropic properties and incorporates a number of nonclassical features. Results reveal that a combination of structural tailoring and control using adaptive materials can play a major role in enhancing the vibrational and static aeroelastic response characteristics of aircraft wings.

I. Introduction

BECAUSE of their outstanding properties, such as high strength/stiffness to weight ratios, fiber-reinforced laminated thick/thin-walled structures are likely to play an increasing role in the design of advanced aircraft wings. In addition, a number of elastic couplings resulting from anisotropy and the ply-angle sequence of composite material structures can be exploited so as to enhance the response characteristics. In this regard, within the last two decades, a technique referred to as structural tailoring has been used with spectacular results.[1] It should be noted, however, that structural tailoring is a passive design technique. This implies that the structure cannot respond adaptively to changes in its parameters or external stimuli. To overcome this shortcoming, additional capabilities must be built into the structure. This is particularly true in view of the fact that future generations of flight vehicles are likely to operate under increasingly severe conditions.

An approach showing good promise is based upon the incorporation into the structure of materials featuring sensing and actuating capabilities.[2–5] Piezoelectric materials are excellent candidates for the role of sensors and actuators. In contrast to passive structures, in which the vibrational and aeroelastic response characteristics are predetermined, in adaptive structures these characteristics can be altered in a known and predictable manner. These adaptive capabilities can be used to prevent structural resonance and/or any other type of instability, as well as to improve the static and dynamic response of the structure.

In this article, the task of enhancing the static aeroelastic response and free vibration characteristics of aircraft wing-type structures made of advanced composite materials is accomplished through the synergistic combination of structural tailoring and adaptive materials technology. The structure simulating the aircraft wing consists of a thin/thick-walled closed cross-sectional cantilevered beam whose constituent layers feature elastic anisotropic properties. The control capability is achieved by electrically actuating piezoelectric elements via the converse piezoelectric effect. The induced localized strain field produces a change in the dynamic characteristics of the structure.

The global constitutive equations of wing structures made of advanced composite materials and incorporating adaptive capabilities are first derived. These adaptive capabilities are provided by piezoelectric layers bonded or embedded into the structure and serving both as sensors and actuators. Then, based on related work,[6] the equations of motion and the associated boundary conditions for composite adaptive structures are derived. Feedback control laws relating the applied electric field to the mechanical response characteristics of the structure are implemented, thus obtaining desired response characteristics. The obtained results underline the fact that the simultaneous implementation of tailoring and adaptive materials technology can enhance the static aeroelastic response and dynamic characteristics of flight vehicle structures significantly.

II. Structural Model

A structural model consisting of a thin-walled beam of arbitrary cross section intended to simulate the lifting surface of advanced flight vehicles is used. Two systems of coordinates, namely s, z, n and x, y, z, are used to describe the kinematics of thin-walled beams, as shown in Fig. 1, with the z axis coinciding with the locus of symmetrical points of the cross sections along the wingspan. The theory of thin-walled beams used herein incorporates the following nonclassical features: 1) anisotropy of constituent material layers, 2) transverse shear and 3) primary and secondary warping effects. In the light of 2, the structural model applies not only to thin-walled beams, but also to thick-walled beams. The theory is based also on the in-plane cross-sectional nondeformability assumption.[7–9]

Consistent with the previous statements, the components of the displacement vector are expressed as

$$u(x, y, z, t) = u_0(z, t) - y\phi(z, t) \tag{1a}$$

$$v(x, y, z, t) = v_0(z, t) + x\phi(z, t) \tag{1b}$$

$$w(x, y, z, t) = w_0(z, t) + \theta_x(z, t)[y(s) + nm] + \theta_y(z, t)[x(s) + nl] - \phi'(z, t)[F_\omega(s) + na(s)] \tag{1c}$$

where $l = \cos(n, x)$ and $m = \cos(n, y)$ denote the direction cosines. In addition

$$\theta_x(z, t) = \gamma_{yz}(z, t) - v_0'(z, t) \tag{2a}$$

$$\theta_y(z, t) = \gamma_{xz}(z, t) - u_0'(z, t) \tag{2b}$$

Received Oct. 4, 1993; revision received June 23, 1995; accepted for publication July 5, 1995.

*Professor, Department of Engineering Science and Mechanics.
†University Distinguished Professor, Department of Engineering Science and Mechanics. Fellow AIAA.
‡Research Associate, Department of Engineering Science and Mechanics; currently Associate Professor, Choong-Nam National University, Mechanical Engineering Department, Taejon 305-764, Republic of Korea.

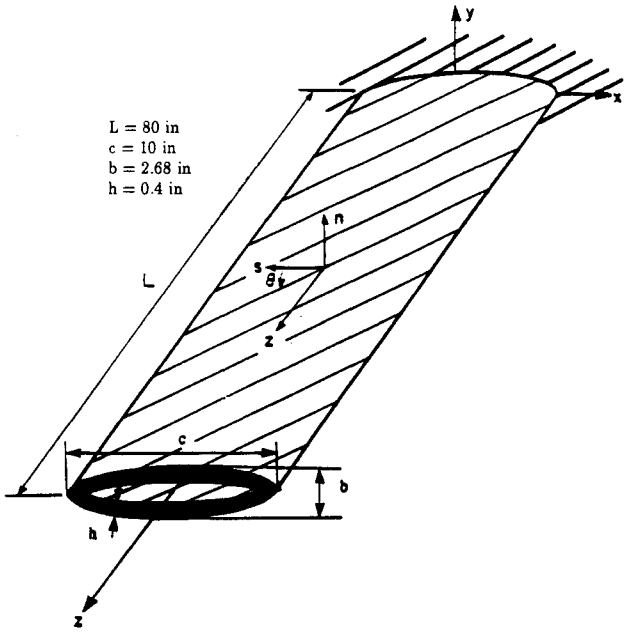

Fig. 1 Thin-walled cantilever beam.

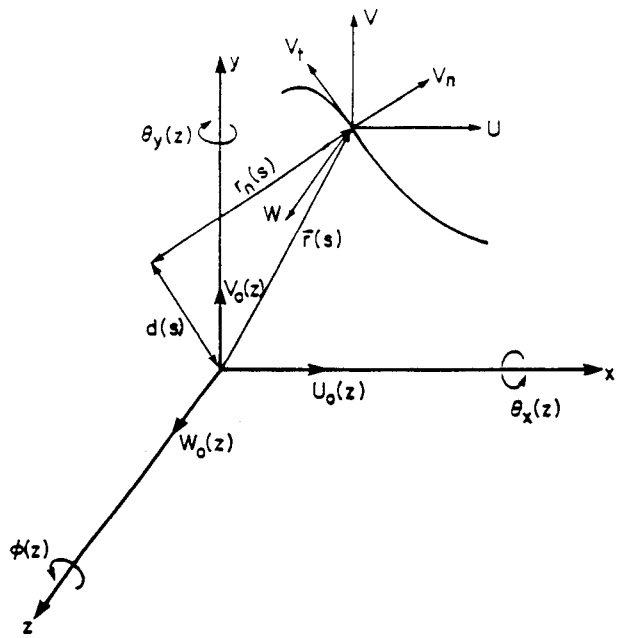

Fig. 2 Displacement field and coordinate systems.

where $\theta_x(z, t)$ and $\theta_y(z, t)$ denote the rotations about axes x and y, respectively, whereas γ_{yz} and γ_{xz} denote the transverse shear strains in the planes yz and xz, respectively. Based on Eqs. (1), the axial strain component reduces to

$$S_{zz}(n, s, z, t) = \bar{S}_{zz}(s, z, t) + n\bar{\bar{S}}_{zz}(s, z, t) \tag{3}$$

where

$$\bar{S}_{zz}(s, z, t) = w_0'(z, t) + \theta_y'(z, t)x(s) + \theta_x'(z, t)y(s) - \phi''(z, t)F_\omega(s) \tag{4a}$$

$$\bar{\bar{S}}_{zz}(s, z, t) = \phi_y'(z, t)l + \theta_x'(z, t)m - \phi''(z, t)a(s) \tag{4b}$$

are the axial strains associated with the primary and secondary warping, respectively, in which primes denote derivatives with respect to z. The membrane and transverse shear strain components can be expressed in the form

$$S_{sz}(s, z, t) = \bar{S}_{sz}(s, z, t) + 2(A_C/\beta)\phi'(z, t) \tag{5}$$

$$S_{nz}(s, z, t) = [\theta_y(z, t) + u_0'(z, t)]l + [\theta_x(z, t) + v_0'(z, t)]m \tag{6a}$$

respectively, where

$$\bar{S}_{sz}(s, z, t) = -[\theta_y(z, t) + u_0'(z, t)]m + [\theta_x(z, t) + v_0'(z, t)]l \tag{6b}$$

In the previous equations, $u_0(z, t)$, $v_0(z, t)$, and $w_0(z, t)$ represent rigid-body translations in the x, y, and z directions, and $\phi(z, t)$ represents the twist about the z axis (see Fig. 2). Moreover, $h = h(s)$ denotes the wall thickness, allowed to vary in the circumferential direction, A_C is the cross-sectional area bounded by the contour midline, β is the total length of the contour midline, and t is the time. In addition, $F_\omega(s)$ denotes the warping function defined as[6-9]

$$F_\omega(s) = \int_0^s [r_n(s) - \psi]\, ds \tag{7}$$

where

$$\psi = \frac{\oint \frac{r(s)}{h(s)}\, ds}{\oint \frac{1}{h(s)}\, ds} = \frac{2A_C}{\beta} \tag{8}$$

is the torsional function, in which $\oint(\cdot)\, ds$ denotes the integral along the closed midline contour, and $r_n(s)$ and a are geometric quantities defined as

$$r_n(s) = x(s)l + y(s)m, \qquad a = xm - yl \tag{9}$$

When the structure exhibits infinite rigidities in transverse shear, $\theta_y(z, t) \to -u_0'(z, t)$ and $\theta_x(z, t) \to -v_0'(z, t)$.

III. Constitutive Equations for Adaptive Wings

As recently demonstrated,[2-5,10,11] controls by means of piezoelectric devices can enhance significantly the response characteristics of structures. Piezoelectric materials, integrated into the load-bearing structure by means of surface bonding or embedding, serve as networks of actuator/sensor systems.

The linear three-dimensional piezoelectric constitutive equations can be expressed in contracted index notation[12]

$$\sigma_i = C_{ij}^{\mathrm{E}} S_j - e_{ki}\mathrm{E}_k \tag{10a}$$

$$D_k = e_{kj}S_j + \varepsilon_{kl}^{S}\mathrm{E}_l \tag{10b}$$

where σ_i and S_j ($i, j = 1, 2, \ldots, 6$) denote the stress and strain components, respectively, in which

$$S_j = \begin{cases} S_{pr} & \text{for } p = r, \quad j = 1, 2, 3 \\ 2S_{pr} & \text{for } p \neq r, \quad j = 4, 5, 6 \end{cases} \tag{11}$$

Moreover, C_{ij}^{E}, e_{ki}, and ε_{kl}^{S} are the elastic (measured under constant electric field), piezoelectric, and dielectric constants (measured under constant strain), whereas E_k and D_k ($k = 1, 2, 3$) denote the electric field intensity and electric displacement vector, respectively. Summation over repeated indices is implied in Eqs. (10). Equations (10a) and (10b) describe the converse and direct piezoelectric effects, respectively.

In piezoelectric adaptive structures, the direct effect is used for sensing and the converse effect is used to generate control forces. Equations (10) are valid for the most general anisotropic case, i.e., for triclinic crystals. In the following, the piezoelectric anisotropy is restricted to the case of hexagonal symmetry, the n axis being an axis of rotary symmetry coinciding with the direction of polarization[12] (thickness polarization). In this case, the piezoelectric continuum is characterized by a reduced number of elastic, piezoelectric, and dielectric coefficients. We also assume that the electric field vector $\mathbf{E}_l$ is defined by the component E_3 only, $E_1 = E_2 = 0$, and that the electric field intensity E_3 is uniform over the cross section of the beam. Because of the fact that the voltage is distributed uniformly, we assume that in the static case E_3 is constant, whereas in the dynamic case it depends on time alone. The piezoelectric actuators are distributed over the entire span and their distribution in the circumferential and transversal directions is defined by

$$R_k(n) = H[n - n_{(k-)}] - H[n - n_{(k+)}] \tag{12a}$$

$$R_k(s) = H[s - s_{(k-)}] - H[s - s_{(k+)}] \tag{12b}$$

in which H denotes the Heaviside unit step function. It is assumed that the host structure consists of r layers exhibiting general-type orthotropy and the actuators consist of p piezoelectric layers exhibiting hexagonal symmetry.

Before we derive the one-dimensional global constitutive equations for adaptive wing structures, it will prove convenient to derive the two-dimensional counterparts. Integrating the actual three-dimensional constitutive equations over the wall thickness and assuming that the hoop stress-resultant N_{ss} is negligibly small when compared with the remaining stresses, one obtains the two-dimensional constitutive equations

$$\begin{bmatrix} N_{zz} \\ N_{sz} \end{bmatrix} = \begin{bmatrix} K_{11} & K_{12} & K_{13} & K_{14} \\ K_{21} & K_{22} & K_{23} & K_{24} \end{bmatrix} \begin{bmatrix} \bar{S}_{zz} \\ \bar{S}_{sz} \\ \phi' \\ \bar{\bar{S}}_{zz} \end{bmatrix} - \begin{bmatrix} N^a_{zz} \\ 0 \end{bmatrix} \tag{13}$$

$$N_{zn} = A_{44} S_{zn} \tag{14}$$

$$\begin{bmatrix} L_{zz} \\ L_{sz} \end{bmatrix} = \begin{bmatrix} K_{41} & K_{42} & K_{43} & K_{44} \\ K_{51} & K_{52} & K_{53} & K_{54} \end{bmatrix} \begin{bmatrix} \bar{S}_{zz} \\ \bar{S}_{sz} \\ \phi' \\ \bar{\bar{S}}_{zz} \end{bmatrix} - \begin{bmatrix} L^a_{zz} \\ 0 \end{bmatrix} \tag{15}$$

where N_{zz} and N_{sz} denote tangential stress resultants, N_{zn} denote the transverse shear stress resultant, and L_{zz} and L_{sz} denote the stress couples, all quantities depending on s, z, and t. Moreover, K_{ij} denote the modified local stiffness coefficients listed in the Appendix, and N^a_{zz} and L^a_{zz} denote the piezoelectrically induced-stress resultant and stress couple, respectively, expressed as

$$N^a_{zz}(s, t) = \left(1 - \frac{A_{12}}{A_{11}}\right) \sum_{k=1}^{p} \mathrm{E}_3^{(k)}(t)[n_{(k+)} - n_{(k-)}] e_{31}^{(k)} R_{(k)}(s) \tag{16a}$$

$$L^a_{zz}(s, t) = \sum_{k=1}^{p} \mathrm{E}_3^{(k)}(t) R_{(k)}(s)[n_{(k+)} - n_{(k-)}] e_{31}^{(k)} \times \left\{ \frac{1}{2} \underline{[n_{(k+)} + n_{(k-)}]} - \frac{B_{12}}{A_{11}} \right\} \tag{16b}$$

where, in the case of symmetrically located piezoactuators, the underscored term vanishes.

IV. Equations of Motion for Adaptive Wing Structures

From Ref. 6, the one-dimensional stress-resultants and stress couples are given by

$$T_z(z, t) = \oint N_{zz}\, ds \tag{17a}$$

$$Q_x(z, t) = \oint (-N_{sz} m + N_{zn} l)\, ds \tag{17b}$$

$$Q_y(z, t) = \oint (N_{sz} l + N_{zn} m)\, ds \tag{17c}$$

$$M_x(z, t) = \oint (y N_{zz} + L_{zz} m)\, ds \tag{17d}$$

$$M_y(z, t) = \oint (x N_{zz} + L_{zz} l)\, ds \tag{17e}$$

$$M_z(z, t) = \oint N_{sz} \frac{2A_C}{\beta}\, ds \tag{17f}$$

$$B_\omega(z, t) = \oint [F_\omega(s) N_{zz} + a(s) L_{zz}]\, ds \tag{17g}$$

where T_z is the axial force, Q_x and Q_y are shear forces, and M_x, M_y, and M_z are the bending and twist moments, while B_ω is a bimoment global quantity. In view of Eqs. (13) and (15), the one-dimensional stress measures T_z, M_x, M_y, and B_ω can be cast in the more convenient form

$$T_z = \hat{T}_z - \hat{\hat{T}}_z \tag{18a}$$

$$M_x = \hat{M}_x - \hat{\hat{M}}_x \tag{18b}$$

$$M_y = \hat{M}_y - \hat{\hat{M}}_y \tag{18c}$$

$$B_\omega = \hat{B}_\omega - \hat{\hat{B}}_\omega \tag{18d}$$

where single and double overcarets identify purely mechanical and piezoelectrically induced terms, respectively.

For reasons that will become evident later, we display the expression of M_x only

$$\hat{\hat{M}}_x = \oint \sum_{k=1}^{p} \mathrm{E}_3^{(k)}[n_{(k+)} - n_{(k-)}] e_{31}^{(k)} R_{(k)}(s) \times \left[y\left(1 - \frac{A_{12}}{A_{11}}\right) - m \frac{B_{12}}{A_{11}} \right] ds + \frac{1}{2} \oint \underline{\left\{ m \sum_{k=1}^{p} \mathrm{E}_3^{(k)}[n^2_{(k+)} - n^2_{(k-)}] e_{31}^{(k)} R_{(k)}(s) \right\} ds} \tag{19}$$

It is noticed that the piezoelectrically induced stress resultants are proportional to the applied electric current E_3. In the case of actuators placed symmetrically throughout the thickness of the beam, the underlined term in Eq. (19) vanishes.

One reason for employing advanced composite materials in flight vehicle design lies in the fact that they permit the use of specific lay-up and fiber orientations so as to induce preferred elastic couplings enhancing the response characteristics. As studies on vibration and subcritical/critical aeroelastic behavior of wing structures reveal,[1,13,14] the bending-twist coupling plays a major role. Additional beneficial effects of this cross coupling have been discussed recently in Ref. 15. In the case of wing structures modeled as thin-walled beams, the ply-angle configuration inducing such an elastic coupling is referred to in Ref. 16 as the circumferentially antisymmetric stiffness configuration and in Ref. 17 as the symmetric configuration. The associated ply-angle distribution is governed by the law (see Fig. 3)

$$\theta(y) = -\theta(-y) \tag{20}$$

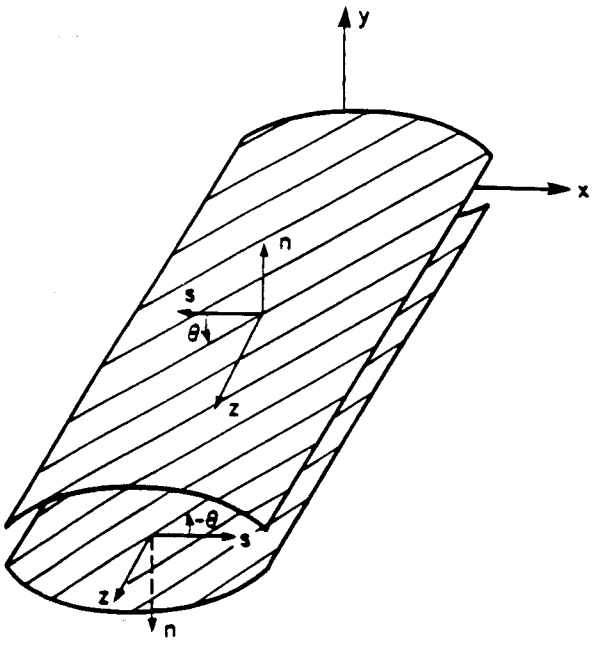

Fig. 3 Circumferentially antisymmetric stiffness configuration, $\theta(y) = -\theta(-y)$.

The resulting equations for adaptive wing structures characterized by the previously mentioned ply-angle configuration are

$$-\underline{a_{66}\phi''''} + a_{73}\theta_x'' - a_{65}(v_0''' + \theta_x'') + a_{77}\phi'' + m_z = (b_4 + b_5)\ddot{\phi} - \underline{(b_{10} + b_{18})\ddot{\phi}''} \tag{21a}$$

$$a_{55}(v_0'' + \theta_x') + \underline{a_{56}\phi'''} + p_y = b_1\ddot{v}_0 \tag{21b}$$

$$a_{33}\theta_x'' + a_{37}\phi'' - a_{55}(v_0' + \theta_x) - \underline{a_{56}\phi''} = (b_4 + b_{14})\ddot{\theta}_x \tag{21c}$$

Moreover, the boundary conditions at $z = 0$ are

$$\phi = 0 \tag{22a}$$

$$\underline{\phi'} = 0 \tag{22b}$$

$$v_0 = 0 \tag{22c}$$

$$\theta_x = 0 \tag{22d}$$

and at $z = L$ they are

$$-\underline{a_{66}\phi'''} + a_{73}\theta_x' + a_{77}\phi' - a_{56}(v_0'' + \theta_x') = -\underline{(b_{10} + b_{18})\ddot{\phi}'} \tag{23a}$$

$$\underline{a_{66}\phi''} + a_{65}(v_0' + \theta_x) = 0 \tag{23b}$$

$$a_{55}(v_0' + \theta_x) + \underline{a_{56}\phi''} = 0 \tag{23c}$$

$$a_{33}\theta_x' + a_{37}\phi' = \hat{\hat{M}}_x \tag{23d}$$

The coefficients appearing in Eqs. (21) and (23) represent stiffness and mass quantities and are given in the Appendix. The existence of two bending–twist stiffness coupling terms, namely, $a_{37} = a_{73}$ and $a_{56} = a_{65}$, should be noted. The latter is induced by the warping restraint effect and its influence is, in general, somewhat less important than that of the former. Their variation with the ply-angle is presented in Fig. 16 of Ref. 6. The singly and doubly dashed underlined terms in Eqs. (21–23) are associated with the warping restraint and warping inertia, respectively. Because the piezoactuators are distributed over the entire wingspan, derivatives with respect to z of piezoelectrically induced terms in Eqs. (21) vanish. This explains why their contribution does not appear in the equations of motion; it appears only as a nonhomogeneous term in the boundary conditions. It should be noticed that $\hat{\hat{M}}_x$ is different from zero only if external voltages of opposite signs are applied in the outer and bottom piezoactuator layer (out-of-phase voltage[18]).

It should be observed here that for the free vibration problem the transverse load p_y and the twisting moment m_z must be ignored in Eqs. (21), and for the static aeroelastic problem the inertia terms must be omitted from Eqs. (21) and (23). Consistent with strip-theory aerodynamics, the unsteady lift force p_y and torsional aerodynamic moment m_z, both per unit span, can be expressed as

$$p_y(z) = q_n c a_0(\phi_0 + \phi - v_0' \tan\Lambda) - NW/2L \tag{24a}$$

$$m_z(z) = q_n c a_0 e(\phi_0 + \phi - v_0' \tan\Lambda) + q_n c^2 C_{MAC} - NWd/2L \tag{24b}$$

Here, $q_n = \frac{1}{2}\rho U_n^2$ denotes the dynamic pressure normal to the leading edge of the swept wing, c is the chord of the wing, a_0 is the "corrected lift" curve slope coefficient, Λ is the angle of sweep (considered positive for sweptback), e is the offset between the aerodynamic and reference axis, ϕ_0 is the rigid angle of attack (measured in planes normal to the leading edge), C_{MAC} is the wing section pitching moment coefficient (whose influence, as usual, is disregarded), $W/2L$ is the weight per unit length of wing, and N is the load factor normal to the wing surface, whose expression is

$$N = \frac{2cq_n a_0}{W}\int_0^L (\phi_0 + \phi - v_0' \tan\Lambda)\, dz \tag{25}$$

The static aeroelastic response is analyzed both in the subcritical range, i.e., for velocities $q_n < (q_n)_D$, and in the critical case as well, where $(q_n)_D$ denotes the divergence dynamic pressure. As a general remark, Eqs. (24) reveal that for $\Lambda < 0$, i.e., for swept-forward wings, the aeroelastic bending-twist coupling results in an increase in $p_y(z)$ and $m_z(z)$, which in turn results in a deterioration of the subcritical static aeroelastic response and in a dramatic decrease of the divergence speed. Whereas the goal of the subcritical static aeroelastic analysis consists of the determination of the distribution of the effective angle of attack ϕ_{eff} and of the lift force, as affected by the elastic deformations, the study of the critical case involves the determination of divergence instability conditions. Clearly, the main target of tailoring applied to swept-forward wings is to yield a decrease in the effective angle of attack, and implicitly in the aeroelastic lift and, as a result, an increase in the critical divergence speed. Whereas the study of the subcritical static aeroelastic response requires the solution of the integral–differential system of equations obtained by inserting Eqs. (24) and (25) into Eqs. (21), the determination of the divergence speed leads to the solution of an eigenvalue problem, where the divergence speed plays the role of eigenvalue. Structural tailoring applied to the vibration of wing structures must result in an increase in the eigenfrequencies without weight penalties. The determination of natural frequencies requires the solution of an eigenvalue problem.[19]

In spite of the mathematical complexities involved in the solution of the previously mentioned problems, in which the eigenvalue appears both in the differential equations and in the boundary conditions, the computational methodologies used proved to be extremely powerful. The spatial Laplace transform method yields exact solutions,[4,14] but it is computationally laborious. On the other hand, the extended Galerkin method yields approximate solutions in excellent agreement with the exact ones and with significantly less computational effort.[20]

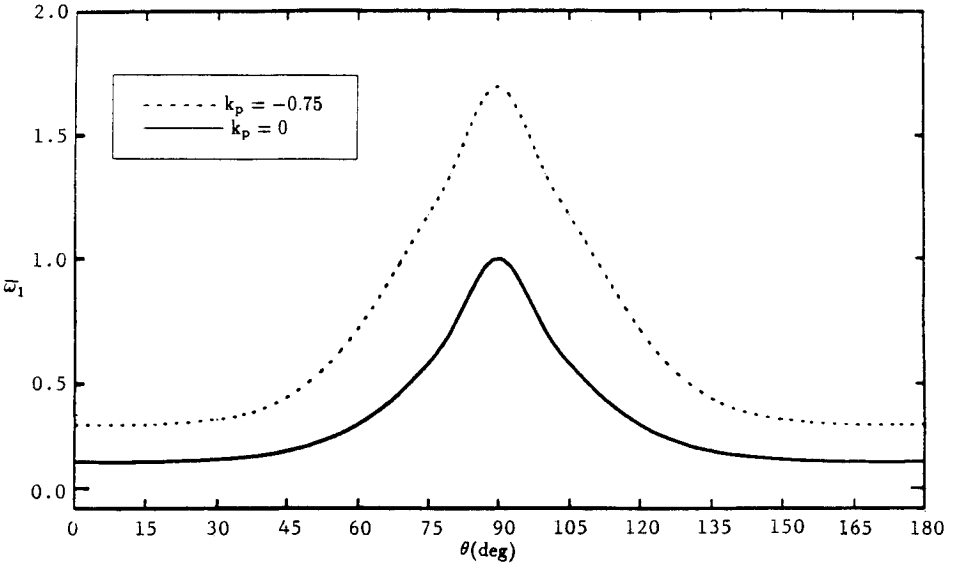

Fig. 4 First normalized coupled eigenfrequency ($\bar{\omega}_1 = \omega_1/\omega_N$) vs the ply angle for the uncontrolled and controlled wing (*CL*1).

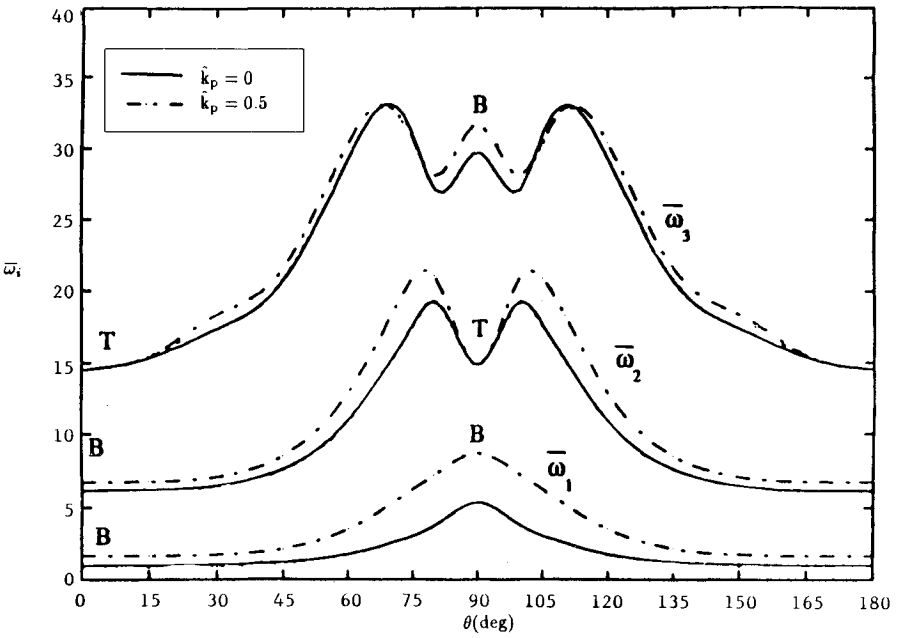

Fig. 5 Three normalized coupled eigenfrequencies ($\bar{\omega}_i = \omega_i/\omega_N$) for various ply angles and for nonactivated ($\hat{k}_p = 0$) and activated wing (*CL*2), ($\omega_N = 44$ rad/s).

V. Control Law and the Closed-Loop Eigenvalues

For feedback control, the applied electric field E_3, which is proportional to the piezoelectrically induced moment, depends on the wing response. Two simple control laws are being considered. The first control law, denoted by *CL*1, requires that the applied electric field E_3 be proportional to the bending moment $\hat{M}_x(0)$ at the wing root, which implies that

$$E_3 = G\theta_x'(0) \tag{26}$$

Upon considering the boundary condition [the last part of Eq. (23)] as well as Eq. (19b), the control law given by Eq. (26) can be rewritten as

$$\theta_x'(L) + f_3\phi'(L) - k_p\theta_x'(0) = 0 \tag{27}$$

where $f_3 = a_{37}/a_{33}$ and k_p denotes the feedback gain, a nondimensional quantity. This control law expresses the fact that the bending moment at the wingtip induced by piezoelectric

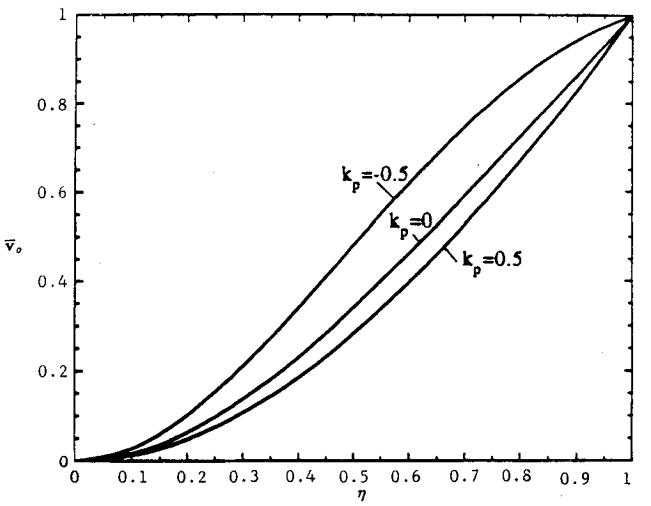

Fig. 6 First normalized mode for the nonactivated ($k_p = 0$) and activated wing ($\theta = 0$ deg, *CL*1).

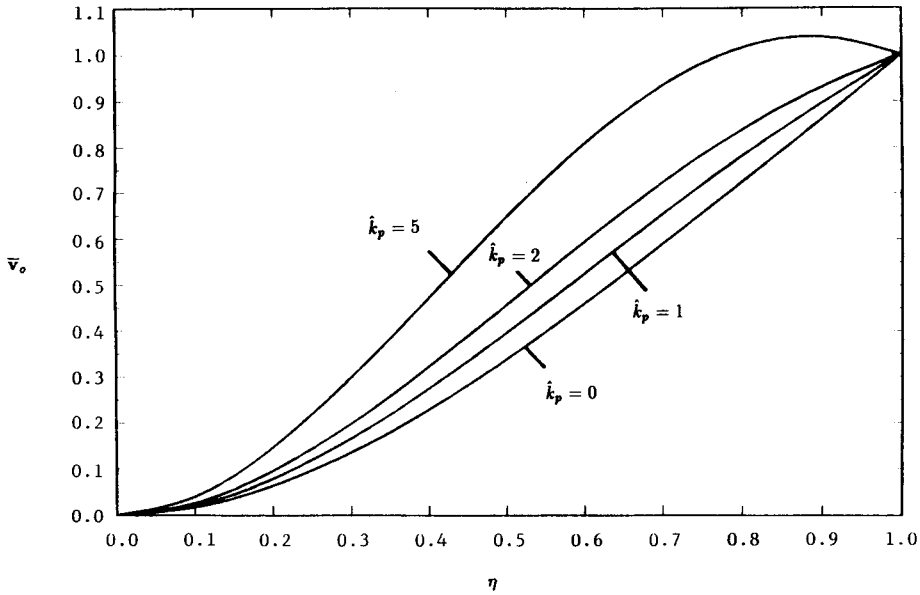

Fig. 7 First normalized mode for several values of the feedback gain (θ = 0 deg, *CL*2).

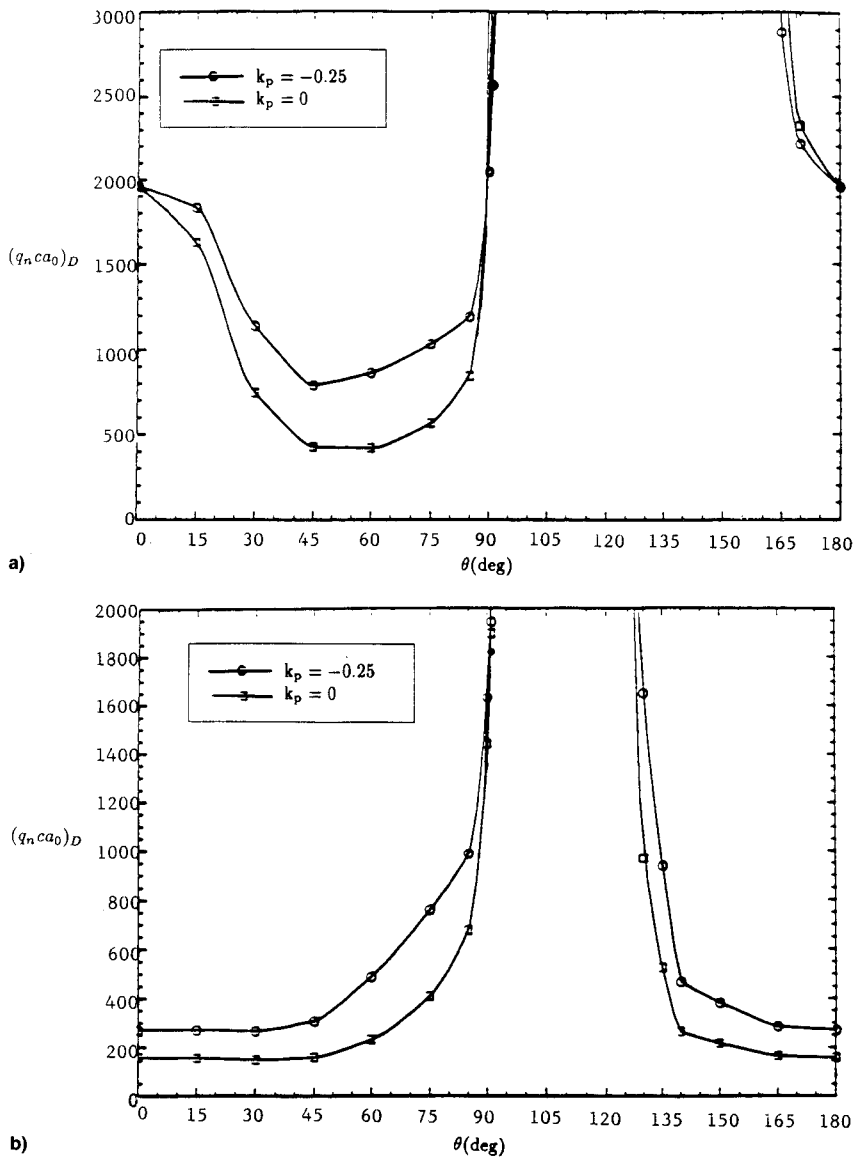

Fig. 8 Divergence speed parameter vs the ply angle for a) uncontrolled and controlled wing (*CL*1), (Λ = 0 deg) and b) nonactivated and activated wing (Λ = −30 deg, *CL*1).

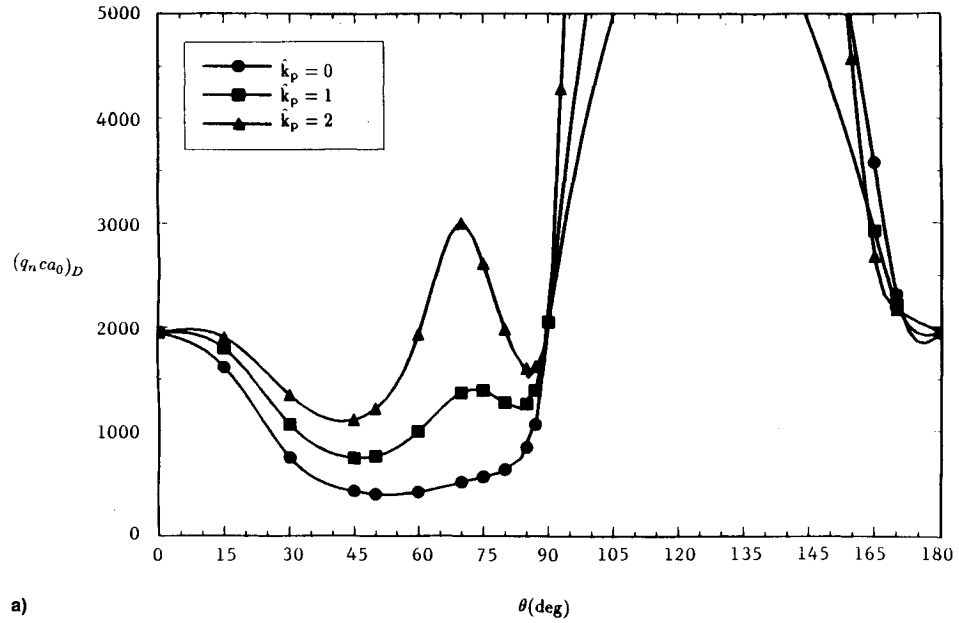

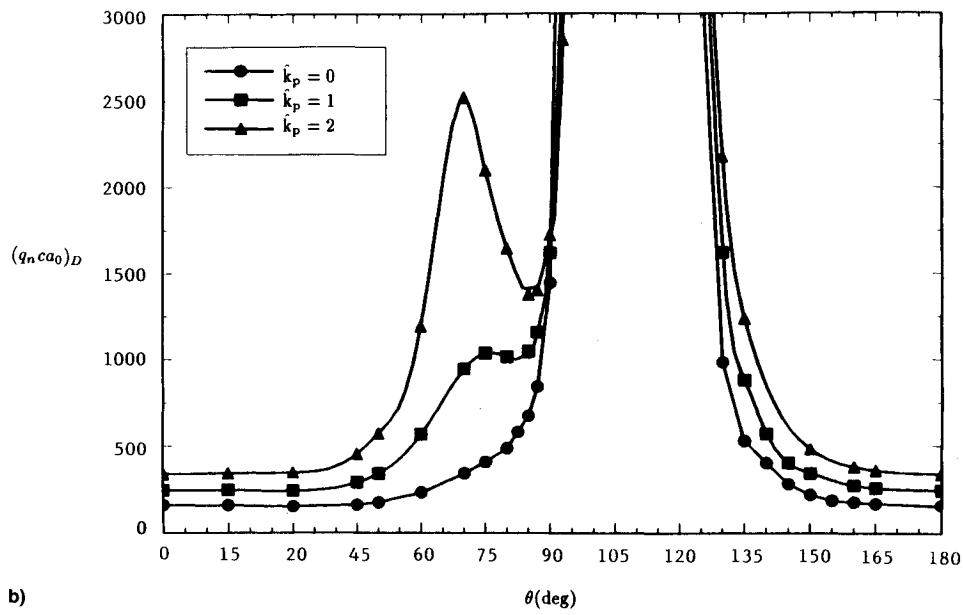

Fig. 9 Divergence speed parameter vs the ply angle for various feedback gains: Λ = a) 0 and b) − 30 deg, *CL2*.

strain actuation is proportional to the mechanical bending moment at the wing root. This control law was used in Refs. 21–23. The second control law, denoted by *CL2*, requires that the applied electric field E_3 be proportional to the vertical deflection of the beam tip $v_0(L)$. This results in the condition

$$\theta_x'(L) + f_3\phi'(L) = \bar{k}_p v_0(L) \tag{28}$$

Equation (28) expresses the fact that the piezoelectrically induced boundary moment control at the wingtip, is proportional to the transverse deflection at the wingtip. Control law (28) is similar to the one proposed and used in Refs. 21, 4, and 24. It should be noted that the feedback gain $\bar{k}_p$ can be nondimensionalized by writing $\hat{k}_p = \bar{k}_p L^2$.

VI. Numerical Examples

The equations derived here are general, in the sense that they are valid for a beam of arbitrary cross section, as well as for piezoelectric actuators arbitrarily located throughout the wall thickness and along the circumference of the beam. However, in the present case a biconvex profile, typical of supersonic wing airplanes, is adopted. It is assumed that the piezoceramic actuators used here are mounted symmetrically on the upper and bottom surfaces of the wing. The host structure is assumed to be of a graphite/epoxy material whose elastic characteristics are

$$E_L = 30 \times 10^6 \text{ psi}, \qquad E_T = 0.75 \times 10^6 \text{ psi}$$

$$G_{LT} = 0.37 \times 10^6 \text{ psi}, \qquad G_{TT} = 0.45 \times 10^6 \text{ psi}$$

$$\mu_{TT} = \mu_{LT} = 0.25, \qquad \rho = 14.3 \times 10^{-5} \text{ lbs}^2/\text{in.}^4$$

where the subscripts L and T denote directions parallel and transversal to the fibers, respectively. The geometrical wing characteristics are displayed in Fig. 1, and the properties of the piezoelectric actuators, made of PZT-4 ceramic, are given in Ref. 25.

The associated differential eigenvalue problem has been discretized in space by the extended Galerkin method.[20] The obtained results were checked by means of an exact solution methodology based on a spatial Laplace transform[14,26] and the agreement was found to be excellent.

Structural tailoring and adaptive material technology are applied simultaneously to enhance the vibrational characteristics of wing structures. Results are displayed in Figs. 4 and Fig. 5 for the control laws $CL1$ and $CL2$, respectively. It should be mentioned that, for $\theta \neq 0$ and $\theta \neq 90$ deg, the bending–twist coupling causes the control to be somewhat weaker in places where the twist is very strong. On the other hand, for $\theta = 0$ and 90 deg, where the bending decouples, the control becomes very effective. As a rule, the frequencies were normalized with respect to the ones corresponding to the uncontrolled case $k_p = 0$ and to on-axes ply angle configuration $\theta = 0$. The trend in the eigenfrequencies using $CL2$ agrees fully with one obtained theoretically and verified experimentally in Ref. 24. As can be concluded from Fig. 5, the first eigenfrequency changes gradually with the ply angle from one corresponding to a pure bending mode (labeled as B) at $\theta = 0$ to a coupled bending–twist mode for $0 < \theta < 90$ deg and to a pure bending mode for $\theta = 90$ deg. On the other hand, the second eigenfrequency changes from a pure bending mode at $\theta = 0$ to a pure twist mode (labeled as T) for $\theta = 90$ deg, and the third eigenfrequency changes from pure twist for $\theta = 0$ to pure bending for $\theta = 90$ deg.

Plots of the closed-loop first mode obtained via $CL1$ and $CL2$ are shown in Figs. 6 and 7, respectively. It clearly appears that the original uncontrolled modes differ considerably from the controlled modes. However, for the higher modes, the control via $CL2$ appears to be less efficient as compared with $CL1$. In Figs. 8a and 8b and 9a and 9b, the reduced divergence speed parameter $(q_n c a_0)_D$ is displayed as a function of θ for various values of the feedback gain using $CL1$ and $CL2$ for the cases of a straight wing $\Lambda = 0$, and a swept-forward wing $\Lambda = -30$ deg. As readily seen, the use of both tailoring and adaptive material control with negative and positive feedback gains using $CL1$ and $CL2$, respectively, results in a significant increase in the divergence speed. Figures 9a and 9b reveal, moreover, that in the region where the bending–twist cross coupling attains a maximum value, i.e., around $\theta \cong 65$ deg, a strong increase in the divergence speed is experienced with the increase of the feedback gain. Beyond that specific value of θ, and irrespective of the values of the feedback gain, the divergence speed follows closely the variation of the uncontrolled wing, where tailoring attains maximum efficiency. In Figs. 10a and 10b and 11a and 11b, the normalized effective angle of attack ϕ_{eff}/ϕ_0 using $CL1$ and $CL2$, in conjunction

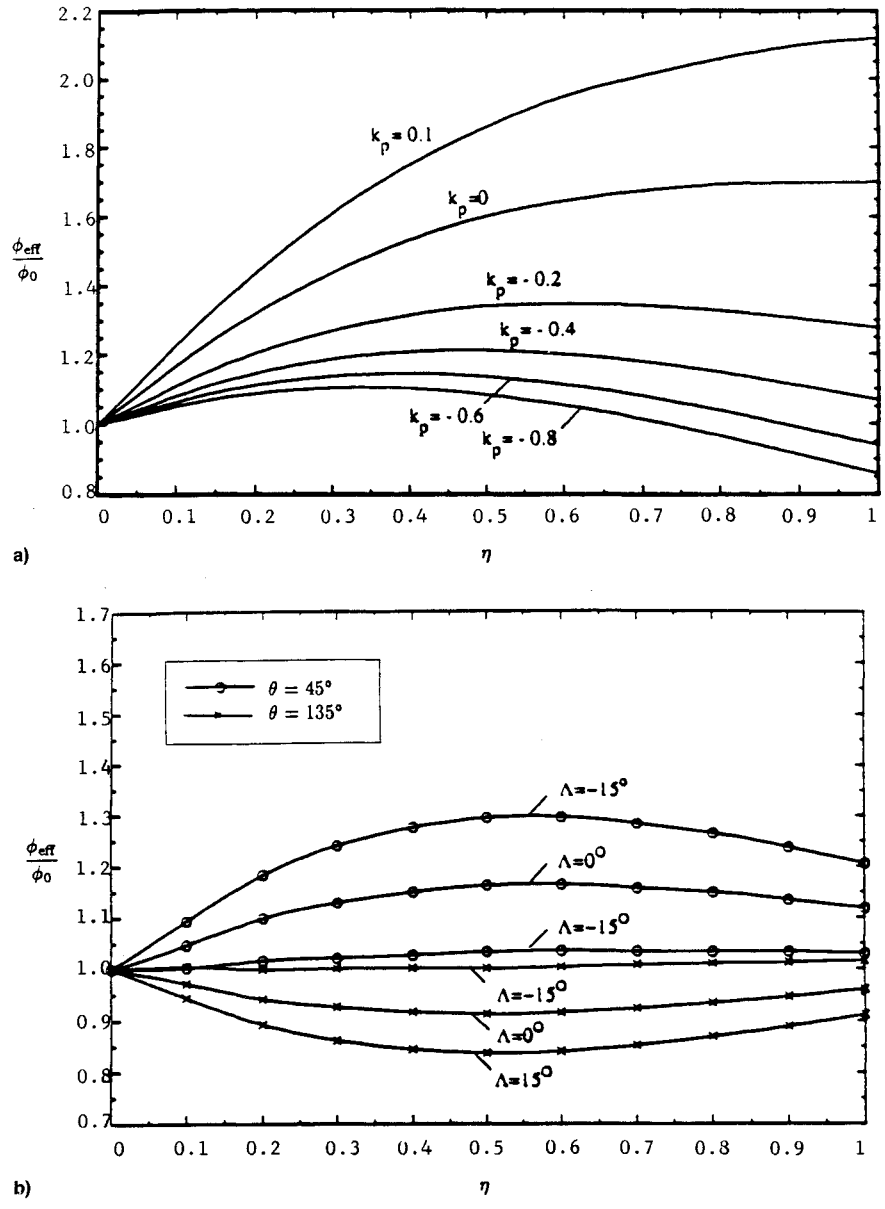

Fig. 10 Distribution of the effective normalized angle of attack along the wing span for a) various feedback gains ($\Lambda = -15$ deg, $\theta = 45$ deg, $q_{\text{flight}} = 2$ psi, $CL1$) and b) three sweep angles ($k_p = 0.25$, $\theta = 45$ deg, 135 deg, $q_{\text{flight}} = 2$ psi, $CL1$).

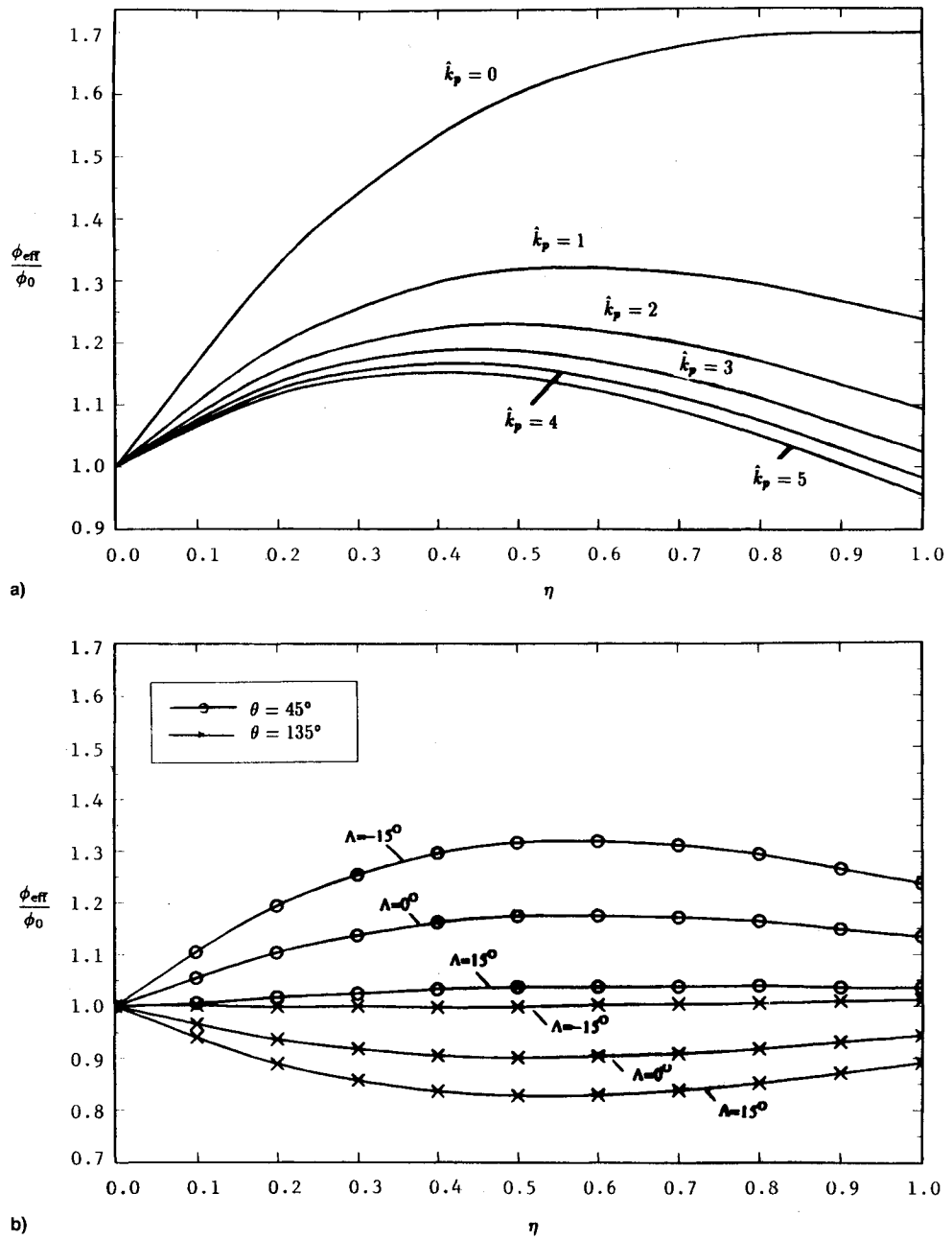

Fig. 11 Distribution of the effective normalized angle of attack along the wingspan for a) various feedback gains ($\Lambda = -15$ deg, $\theta = 45$ deg, $q_{\text{flight}} = 2$ psi, *CL2*) and b) three sweep angles ($\hat{k}_p = 1$, $q_{\text{flight}} = 2$ psi, *CL2*).

with various control gains, is displayed. The results reveal that strong attenuations of aeroelastic loads are experienced for both $k_p < 0$ and $k_p > 0$ as compared to the uncontrolled wing ($k_p = 0$). As Fig. 11 reveals, as the magnitude of the feedback gain increases, the attenuation becomes more and more pronounced.

The results demonstrate that the use of both tailoring and adaptive control techniques can yield dramatic improvements in the dynamic and static aeroelastic characteristics of aircraft wings.

VII. Summary and Conclusions

A comprehensive structural model of aircraft wing modeled as a thin/thick-walled beam of arbitrary closed cross section, incorporating adaptive capabilities via the converse piezoelectric effect was developed. The anisotropic wing model incorporates a number of nonclassical features characteristic of advanced wing structures. It is demonstrated here that the synergistic effect resulting from the simultaneous use of tailoring of anisotropic composite materials, through the implementation of a proper ply-angle configuration and control by means of adaptive materials, produces a wing with better dynamic and static aeroelastic characteristics than would have been produced with either tailoring or control alone. Incorporation of both technologies can provide an expanded performance envelope of flight vehicles, without weight penalties.

Appendix: Stiffness Coefficients

The modified local stiffness coefficients are

$$K_{11} = A_{22} - \frac{A_{12}^2}{A_{11}} \tag{A1}$$

$$K_{12} = A_{26} - \frac{A_{12}A_{16}}{A_{11}} = K_{21} \tag{A2}$$

$$K_{13} = 2K_{12}\frac{A_c}{\beta} \tag{A3}$$

$$K_{14} = B_{22} - \frac{A_{12}B_{12}}{A_{11}} = K_{41} \tag{A4}$$

$$K_{22} = A_{66} - \frac{A_{16}^2}{A_{11}} \tag{A5}$$

$$K_{23} = 2K_{22}\frac{A_c}{\beta} \tag{A6}$$

$$K_{24} = B_{26} - \frac{A_{16}B_{12}}{A_{11}} = K_{42} \tag{A7}$$

$$K_{43} = 2K_{24}\frac{A_c}{\beta} \tag{A8}$$

$$K_{44} = D_{22} - \frac{B_{12}^2}{A_{11}} \tag{A9}$$

$$K_{51} = B_{26} - \frac{B_{16}A_{12}}{A_{11}} \tag{A10}$$

$$K_{52} = B_{66} - \frac{B_{16}A_{16}}{A_{11}} \tag{A11}$$

$$K_{53} = 2K_{52}\frac{A_c}{\beta} \tag{A12}$$

$$K_{54} = D_{26} - \frac{B_{12}B_{16}}{A_{11}} \tag{A13}$$

where A_{ij}, B_i, and D_{ij} denote, respectively, the stretching, bending-stretching, and bending stiffness quantities associated with the entire structure. The structure consists of r host and p piezoelectric layers, for a total $N = r + r$.

The global stiffness and mass coefficients have the form

$$a_{11} = \oint K_{11}\,ds \tag{A14}$$

$$a_{14} = a_{41} = -\oint K_{12}m\,ds \tag{A15}$$

$$a_{22} = \oint (K_{11}^2 + 2xK_{14}l + K_{44}l^2)\,ds \tag{A16}$$

$$a_{33} = \oint (K_{11}y^2 + 2yK_{14}m + K_{44}m^2)\,ds \tag{A17}$$

$$a_{37} = a_{73} = \oint (yK_{13} + K_{43}m)\,ds \tag{A18}$$

$$a_{44} = \oint (K_{22}m^2 + A_{44}l^2)\,ds \tag{A19}$$

$$a_{55} = \oint (K_{22}l^2 + A_{44}m^2)\,ds \tag{A20}$$

$$a_{56} = a_{65} = -\oint (F_\omega K_{21}l + K_{24}al)\,ds \tag{A21}$$

$$a_{66} = \oint (K_{11}F_\omega^2 + 2K_{14}F_\omega a + K_{44}a^2)\,ds \tag{A22}$$

$$a_{77} = \oint 2\frac{A_c}{\beta}K_{23}\,ds \tag{A23}$$

$$(b_1, b_4, b_5, b_{10}) = \oint m_0(1, y^2, x^2, F_\omega^2)\,ds \tag{A24}$$

$$(b_{14}, b_{15}, b_{18}) = \oint m_2(m^2, l^2, a^2)\,ds \tag{A25}$$

where

$$(m_0, m_2) = \sum_{k=1}^{N}\int_{h_{(k-1)}}^{h_{(k)}} \rho_{(k)}(1, n^2)\,dn \tag{A26}$$

Acknowledgments

This work was supported by AFOSR Research Grant 91-0351. Technical discussions with Jim C. I. Chang and his constant encouragement are greatly appreciated.

References

[1]Weisshaar, T. A., "Aeroelastic Tailoring—Creative Use of Unusual Materials," AIAA Paper 87-0976, April 1987.

[2]Crawley, E. F., and DeLuis, T., "Use of Piezoelectric Actuators as Elements of Intelligent Structures," *AIAA Journal*, Vol. 25, No. 10, 1988, pp. 1373–1385.

[3]Tzou, H. S., and Anderson, G. L. (eds.), *Intelligent Structural Systems*, Kluwer Academic, Norwell, MA, 1992.

[4]Tzou, H. S., *Piezoelectric Shells—Distributed Sensing and Control of Continuum*, Kluwer Academic, Dordrecht, The Netherlands, 1993.

[5]Crawley, E. F., "Intelligent Structures for Aerospace: A Technology Overview and Assessment," *AIAA Journal*, Vol. 31, No. 8, 1994, pp. 1689–1699.

[6]Librescu, L., Meirovitch, L., and Song, O., "Refined Structural Modeling for Enhancing Vibrations and Aeroelastic Characteristics of Composite Aircraft Wings," *La Recherche Aérospatiale*, No. 6, 1995.

[7]Librescu, L., and Song, O., "Behavior of Thin-Walled Beams Made of Advanced Composite Materials and Incorporating Non-Classical Effects," *Applied Mechanics Reviews*, Vol. 44, No. 11, Pt. 2, 1991, pp. 174–180.

[8]Rehfield, L. W., Atilgan, A. R., and Hodges, D. H., "Nonclassical Behavior of Thin-Walled Composite Beams," *Journal of the American Helicopter Society*, Vol. 35, No. 2, 1990, pp. 42–50.

[9]Chandra, R., Stemple, A. D., and Chopra, I., "Thin-Walled Composite Beams Under Bending, Torsional and Extensional Loads," *Journal of Aircraft*, Vol. 27, No. 7, 1990, pp. 619–626.

[10]Lee, C. K., "Piezoelectric Laminates: Theory and Experiments for Distributed Sensors and Actuators," *Intelligent Structural Systems*, edited by H. S. Tzou and G. L. Anderson, Kluwer Academic, Boston, MA, 1992, pp. 75–167.

[11]Hagood, N. W., Crawley, E. F., DeLuis, J., and Anderson, E. H., "Development of Integrated Components for Control of Intelligent Structures," *First Joint U.S./Japan Conference on Adaptive Structures* (Maui, HI), edited by B. K. Wada, J. L. Fanson, and N. Miura, Technomic, Westport, CT, 1990, pp. 80–194.

[12]Eringen, A. C., and Maugin, G. A., *Electrodynamics of Continua I., Foundations and Solid Media*, Springer–Verlag, New York, 1990.

[13]Librescu, L., and Simovich, J., "General Formulation for the Aeroelastic Divergence of Composite Swept Forward Wing Structures," *Journal of Aircraft*, Vol. 25, No. 4, 1988, pp. 364–371.

[14]Librescu, L., and Thangjitham, S., "Analytical Studies on Static Aeroelastic Behavior of Forward-Swept Composite Wing Structures," *Journal of Aircraft*, Vol. 28, No. 2, 1991, pp. 151–157.

[15]Garfinkle, M., "Twisting Smartly in the Wind," *Aerospace America*, July 1994, pp. 18–20.

[16]Rehfield, L. W., and Atilgan, A. R., "Toward Understanding the Tailoring Mechanisms for Thin-Walled Composite Tubular Beams," *Proceedings of the 1st USSR-U.S. Symposium on Mechanics of Composite Materials* (Riga, Latvia), edited by S. W. Tsai, J. M. Whitney, T.-W. Chou, and R. M. Jones, American Society of Mechanical Engineers, New York, 1989, pp. 187–196.

[17]Smith, E. C., and Chopra, I., "Formulation and Evaluation of an Analytical Model for Composite Box-Beams," *Journal of the American Helicopter Society*, Vol. 36, No. 3, 1991, pp. 23–35.

[18]Birman, V., "Analytical Models of Sandwich Plate, with Piezoelectric Strip Stiffeners," *International Journal of Mechanical Science*, Vol. 36, No. 6, 1994, pp. 167–178.

[19]Meirovitch, L., *Computational Methods in Structural Dynamics*,

Sijhoff and Noordhoff Alphen aan den Rijn, The Netherlands, 1980.

[20]Palazotto, A. N., and Linnemann, P. E., "Vibration and Buckling Characteristics of Composite Cylindrical Panels Incorporating the Effects of a Higher Order Shear Theory," *International Journal of Solids and Structures*, Vol. 28, No. 3, 1991, pp. 341–361.

[21]Song, O., Librescu, L., and Rogers, C. A., "Vibrational Behavior of Adaptive Aircraft Wing Structures Modelled as Composite Thin-Walled Beams," *Proceedings of the 9th DoD/NASA/FAA Conference on Fibrous Composites in Structural Design* (Lake Tahoe, NV), Vol. I, DOT/FAA/CT-92-25, 1992, pp. 361–381.

[22]Ehlers, S. M., and Weisshaar, T. A., "Static Aeroelastic Behavior of an Adaptive Laminated Piezoelectric Composite Wing," *Proceedings of the AIAA/ASME/ASCE/AHS 31st Structures, Structural Dynamics and Materials Conference* (Long Beach, CA), AIAA, Washington, DC, 1990, pp. 1611–1623.

[23]Weisshaar, T. A., and Ehlers, S. M., "Adaptive Aeroelastic Composite Wings—Control and Optimization Issues," *Composites Engineering*, Vol. 2, Nos. 5–7, 1992, pp. 457–476.

[24]Tzou, H. S., and Zhong, J. P., "Adaptive Piezoelectric Structures: Theory and Experiment," *Active Materials and Adaptive Structures, Proceedings of the ADPA/AIAA/ASME/SPIE Conference on Active Materials and Adaptive Structures*, edited by G. J. Knowles, AIAA, Washington, DC, 1991, pp. 719–724.

[25]Berlincourt, D. A., Curran, D. R., and Jaffe, H., "Piezoelectric and Piezomagnetic Materials and Their Function in Transducers," *Physical Acoustics—Principles and Methods*, edited by W. P. Mason, Vol. 1, Pt. A, Academic, New York, 1964, pp. 169–270.

[26]Karpouzian, G., and Librescu, L., "A Comprehensive Model for Anisotropic Composite Aircraft Wings Suitable for Aeroelastic Analyses," *Journal of Aircraft*, Vol. 31, No. 3, 1994, pp. 703–712.